

TD-DFT Calculations of One- and Two-Photon Absorption in Coumarin C153 and Prodan: Attuning Theory to Experiment

Merle Uudsemaa,^b Aleksander Trummal,^b Sophie de Reguardati,^b Patrik R. Callis,^c and Aleksander Rebane^{a,b*}

^a Department of Physics, Montana State University, Bozeman, MT 59717, USA

E-mail: arebane@montana.edu

^b Laboratory of Chemical Physics, National Institute of Chemical Physics and Biophysics, 23 Akadeemia tee, Tallinn 12618, Estonia

^c Department of Chemistry and Biochemistry, Montana State University, Bozeman, MT 59717, USA

Electronic Supplementary Information

Table of Contents

Computational details.....	S2
The calculated 1PA/2PA parameters and $\Delta\mu$ values.....	S3
Experimental 1PA spectra with transition energies and oscillator strengths from TD-DFT PCM calculations	S5
Frontier orbitals	S6
Experimental 1PA spectra and deconvolution details.....	S8
Vibronic spectra from FCHT calculations	S10
Fluorescence excitation anisotropy of Prodan	S14
REFERENCES.....	S15

Computational details

The ground state conformational search for the Prodan and C153 was carried out in the gas phase as reported earlier.¹ For the lowest energy conformers of Prodan and syn-C153 full DFT geometry optimization in the gas and solution phases (toluene, DMSO) at the B3LYP^{2,3}/6-311G(d,p)⁴ level was carried out followed by vibrational normal mode analysis to assess the nature of the stationary points. The lack of imaginary eigenvalues in harmonic vibrational spectra was observed for each optimized structure. Therefore, the calculated stationary points represent true minima on the potential energy surface. Solvent effects were included in the framework of the polarized continuum model IEF-PCM^{5,6} as implemented in Gaussian09 package.⁷ The internally stored values for dielectric constants of toluene (2.3741) and DMSO (46.826) were used.

Dalton2015 software suite^{8,9} was used for all one-photon absorption (1PA), two-photon absorption (2PA) and change of the permanent electric dipole moment ($\Delta\mu$) calculations in solvent. The construction of dividing surface between solute cavity and the bulk solvent was based on spheres defined for heavy atoms only to reduce the number of intersections and achieve smoother convergence. This approach was successfully validated by comparison of the respective results with default PCM calculations where one sphere on each individual atom was used.

We used three hybrid functionals, namely B3LYP, PBE0¹⁰ and CAM-B3LYP¹¹ for TD-DFT¹² calculations. Following common practice,¹³⁻¹⁵ the calculations were based on B3LYP optimized geometry. In addition, the popular CAM-B3LYP range-separated hybrid functional with the mild coulombic attenuation has been tuned to test its performance for prediction of 1PA properties depending on the choice of internal parameters.

As have been reported on several occasions,¹⁶⁻¹⁸ the CAM-B3LYP in its default implementation ($\alpha = 0.19$, $\beta = 0.46$) tends to introduce significant errors in prediction of the energies of electronic transitions. One possible reason behind observed deviations was the lack of asymptotic behaviour in the long range limit. Therefore, it was suggested to apply 100% exact Hartree-Fock exchange for the long range part (i.e. to keep $\alpha + \beta = 1$ condition) and also to decrease the value of the range separation parameter μ . The default value for μ is 0.33 while, according to recent reports by Okuno *et al.*¹⁹ and Vivas *et al.*¹⁴, the value of 0.15 provided more reasonable excitation energies.

Thus, the careful tuning of CAM-B3LYP was carried out to reproduce the experimental 1PA maxima wavelengths as exactly as possible. The values of parameter α varied between 0.01 and 0.19 while the value for β was calculated from the asymptotic condition $\alpha + \beta = 1$.

It has been reported²⁰⁻²² that sometimes the experimental shapes of the absorption lines are significantly affected by underlying vibrational modes and the maximum of the absorption band do not coincide with the vertical excitation energies. In this work vibrationally-resolved electronic spectra were also computed for $S_0 \rightarrow S_1$ transitions. The combination of tuned CAM-B3LYP functional and 6-311++G(d,p) basis set was selected for the Franck-Condon Herzberg-Teller (FCHT) calculations. The geometries of ground state and first vertical excitation state were optimized and frequency calculations have been performed in solvent under equilibrium conditions. The 1PA spectrum was generated at $T = 0$ K, and both FC and HT transitions were included. To achieve a good spectrum convergence (at least 89% for Prodan and 98% for C153) a maximum of 10^9 transitions were considered. The FCHT calculations were carried out using Gaussian09 software.

To characterize the changes in electron density related to particular electronic transition the dominant natural transition orbitals (NTOs) in solvent (DMSO) were calculated and visualized using Gaussian09 and GaussView software packages.

The gas-phase 1PA excitation energies, transition moments and oscillator strengths were calculated at TD-DFT (TD/B3LYP/TZVP) and second-order coupled-cluster (CC2)²³ with resolution of identity (ricc2)²⁴ (CC2/def2-TZVPP²⁵⁻²⁷) level of theory. For naphthalene, the SAC-CI^{28,29}/TZVP level3 calculations using direct method were carried out as well. The TD-DFT and SAC-CI calculations were based on Gaussian09 package, while Turbomole version 6.4³⁰ software was used for CC2 calculations.

The calculated 1PA/2PA parameters and $\Delta\mu$ values

Table S1 Calculated spectral properties of dominant $S_0 \rightarrow S_1$ excitation for C153 in DMSO and in toluene.

Solvent	Method	$\lambda_{1PA,max}$ [nm]	f (oscillator strength)	$\Delta\mu$ [D]	δ_{2PA} (transition probabilities)
DMSO	B3LYP/6-311+G(d)	424	0.3787	6.26	7720
	B3LYP/aug-cc-pVDZ	423	0.3783		
	CAM-B3LYP /6-311+G(d)	376	0.4903	6.61	8183
	PBE0 /6-311+G(d)	410	0.4059		
	<i>m</i> CAM-B3LYP ($\alpha=0.03$ $\beta=0.97$ $\mu=0.1$) /6-311+G(d)	447	0.3219		
	<i>m</i> CAM-B3LYP ($\alpha=0.08$ $\beta=0.92$ $\mu=0.1$) /6-311+G(d)	435	0.3483	6.24	
	<i>m</i> CAM-B3LYP ($\alpha=0.19$ $\beta=0.81$ $\mu=0.1$) /6-311+G(d)	410	0.4051	6.44	7904
	<i>m</i> CAM-B3LYP ($\alpha=0.01$ $\beta=0.99$ $\mu=0.125$) / 6-311++G(d,p)	438	0.3386		
	<i>m</i> CAM-B3LYP ($\alpha=0.08$ $\beta=0.92$ $\mu=0.125$) / 6-311++G(d,p)	423	0.3738	6.37	7654
	<i>m</i> CAM-B3LYP ($\alpha=0.03$ $\beta=0.97$ $\mu=0.125$) /6-311+G(d)	433	0.3472		
	<i>m</i> CAM-B3LYP ($\alpha=0.08$ $\beta=0.92$ $\mu=0.125$) /6-311+G(d)	422	0.3723	6.40	7683
	<i>m</i> CAM-B3LYP ($\alpha=0.19$ $\beta=0.81$ $\mu=0.125$) /6-311+G(d)	401	0.4245		
	<i>m</i> CAM-B3LYP ($\alpha=0.03$ $\beta=0.97$ $\mu=0.15$) /6-311+G(d)	419	0.3760	6.46	7704
	<i>m</i> CAM-B3LYP ($\alpha=0.08$ $\beta=0.92$ $\mu=0.15$) /6-311+G(d)	410	0.3988	6.50	
	<i>m</i> CAM-B3LYP ($\alpha=0.19$ $\beta=0.81$ $\mu=0.15$) /6-311+G(d)	392	0.4450		
	<i>m</i> CAM-B3LYP ($\alpha=0.03$ $\beta=0.97$ $\mu=0.40$) /6-311+G(d)	351	0.5460		
	<i>m</i> CAM-B3LYP ($\alpha=0.19$ $\beta=0.81$ $\mu=0.40$) /6-311+G(d)	344	0.5614		
	toluene	B3LYP/6-311+G(d)	408	0.3815	6.74
CAM-B3LYP /6-311+G(d)		362	0.4915	6.64	7389
<i>m</i> CAM-B3LYP ($\alpha=0.08$ $\beta=0.92$ $\mu=0.125$) /6-311+G(d)		405	0.3789	6.72	7493
<i>m</i> CAM-B3LYP ($\alpha=0.08$ $\beta=0.92$ $\mu=0.125$) / 6-311++G(d,p)		406	0.3807	6.67	7439
<i>m</i> CAM-B3LYP ($\alpha=0.03$ $\beta=0.97$ $\mu=0.15$) /6-311+G(d)		402	0.3839	6.70	7375

Table S2 Calculated spectral properties of dominant $S_0 \rightarrow S_1$ excitation for Prodan in DMSO and in toluene.

Solvent	Method	$\lambda_{1PA,max}$ [nm]	f (oscillator strength)	$\Delta\mu$ [D]	δ_{2PA} (transition probabilities)
DMSO	B3LYP/6-311+G(d)	384	0.5039	8.64	15900
	CAM-B3LYP /6-311+G(d)	333	0.5332	7.35	9578
	PBE0 /6-311+G(d)	370	0.5192		
	<i>m</i> CAM-B3LYP ($\alpha=0.03$ $\beta=0.97$ $\mu=0.15$) /6-311+G(d)	375	0.4215		
	<i>m</i> CAM-B3LYP ($\alpha=0.08$ $\beta=0.92$ $\mu=0.15$) /6-311+G(d)	366	0.4382	7.64	10700
	<i>m</i> CAM-B3LYP ($\alpha=0.19$ $\beta=0.81$ $\mu=0.15$) /6-311+G(d)	349	0.4712		
	<i>m</i> CAM-B3LYP ($\alpha=0.08$ $\beta=0.92$ $\mu=0.15$) /6-311++G(d,p)	367	0.4267	7.57	10400
	<i>m</i> CAM-B3LYP ($\alpha=0.12$ $\beta=0.88$ $\mu=0.15$) /6-311++G(d,p)	361	0.4388	7.50	10000
	<i>m</i> CAM-B3LYP ($\alpha=0.15$ $\beta=0.85$ $\mu=0.15$) /6-311++G(d,p)	356	0.4476	7.44	9796
	<i>m</i> CAM-B3LYP ($\alpha=0.03$ $\beta=0.97$ $\mu=0.175$) /6-311+G(d)	363	0.4242	7.43	9810
	<i>m</i> CAM-B3LYP ($\alpha=0.08$ $\beta=0.92$ $\mu=0.175$) /6-311+G(d)	356	0.4400		
	<i>m</i> CAM-B3LYP ($\alpha=0.19$ $\beta=0.81$ $\mu=0.175$) /6-311+G(d)	341	0.4710		
	<i>m</i> CAM-B3LYP ($\alpha=0.03$ $\beta=0.97$ $\mu=0.175$) /6-311++G(d,p)	364	0.4111		
	<i>m</i> CAM-B3LYP ($\alpha=0.08$ $\beta=0.92$ $\mu=0.175$) /6-311++G(d,p)	357	0.4266	7.28	9180
	<i>m</i> CAM-B3LYP ($\alpha=0.08$ $\beta=0.92$ $\mu=0.175$) /aug-cc-pVDZ	358	0.4079		
	<i>m</i> CAM-B3LYP ($\alpha=0.03$ $\beta=0.97$ $\mu=0.40$) /6-311+G(d)	310	0.5102		
	<i>m</i> CAM-B3LYP ($\alpha=0.19$ $\beta=0.81$ $\mu=0.40$) /6-311+G(d)	305	0.5292		
toluene	B3LYP/6-311+G(d)	371	0.4503	8.57	13200
	CAM-B3LYP /6-311+G(d)	325	0.4460	6.69	6985
	<i>m</i> CAM-B3LYP ($\alpha=0.08$ $\beta=0.92$ $\mu=0.15$) /6-311+G(d)	356	0.3721	7.21	8081
	<i>m</i> CAM-B3LYP ($\alpha=0.08$ $\beta=0.92$ $\mu=0.15$) /6-311++G(d,p)	357	0.3599	7.10	7731
	<i>m</i> CAM-B3LYP ($\alpha=0.15$ $\beta=0.85$ $\mu=0.15$) /6-311++G(d,p)	347	0.3753	6.91	7208
	<i>m</i> CAM-B3LYP ($\alpha=0.03$ $\beta=0.97$ $\mu=0.175$) /6-311+G(d)	353	0.3545	6.93	7230
	<i>m</i> CAM-B3LYP ($\alpha=0.08$ $\beta=0.92$ $\mu=0.175$) /6-311++G(d,p)	347	0.3528	6.70	6624

Experimental 1PA spectra with transition energies and oscillator strengths from TD-DFT PCM calculations

The experimental linear absorption spectra in DMSO along with corresponding stick spectra from PCM/*m*CAM-B3LYP/6-311++G(d,p) calculations are presented in **Figure S1** and **Figure S2** for C153 and Prodan, respectively. For C153 the results from PCM/B3LYP/6-311++G(d,p) calculation are also included for comparison. Only transitions with calculated oscillator strengths above 0.005 are shown out of 10 vertical excitations calculated for each case.

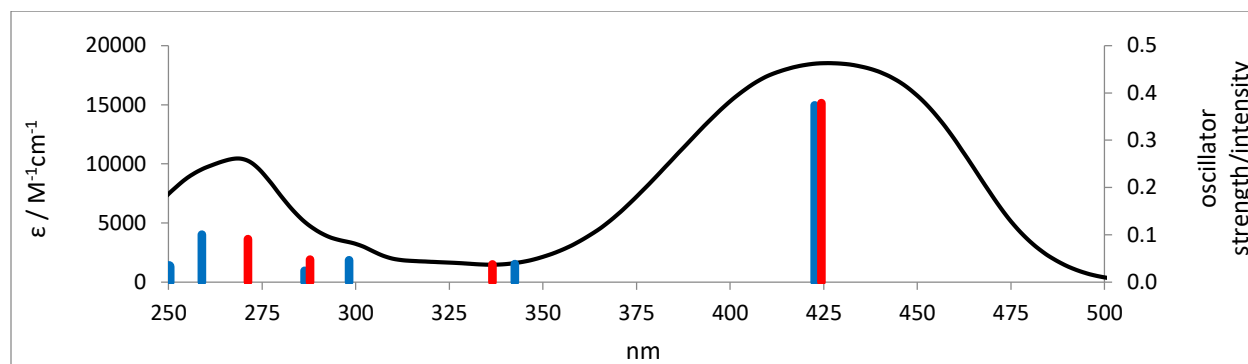


Figure S1 Experimental 1PA spectrum of C153 in DMSO (black line) with transition energies and oscillator strengths from B3LYP (red sticks) and *m*CAM-B3LYP ($\alpha=0.08$ $\beta=0.92$ $\mu=0.125$, blue sticks) calculations at 6-311++G(d,p) level

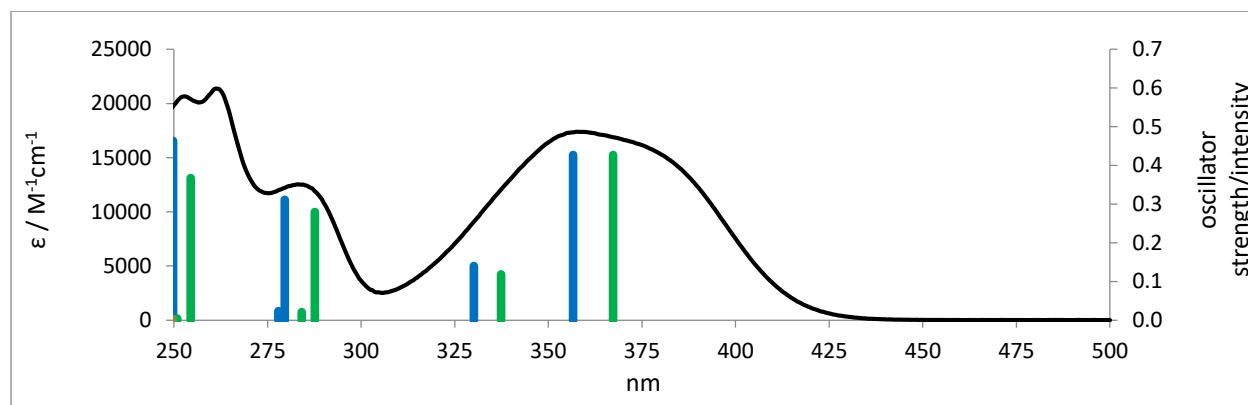


Figure S2 Experimental 1PA spectrum of Prodan in DMSO (black line) with transition energies and oscillator strengths from PCM/*m*CAM-B3LYP ($\alpha=0.08$ $\beta=0.92$ $\mu=0.175$, blue sticks) and PCM/*m*CAM-B3LYP ($\alpha=0.08$ $\beta=0.92$ $\mu=0.15$, green sticks) calculations at 6-311++G(d,p) level

It is worth mentioning that the reasonable match is observed not only for the low-lying transitions but for the 240 to 300 nm range as well, although the latter should be interpreted with some caution.

Frontier orbitals

We used natural transition orbitals (NTO) to analyse the spatial distribution of the orbitals involved in electronic excitations in the low-energy region. The hole (left) and particle (right) NTOs for the dominant transitions from TD-DFT calculations in DMSO are presented in **Figure S3** and **Figure S4**.

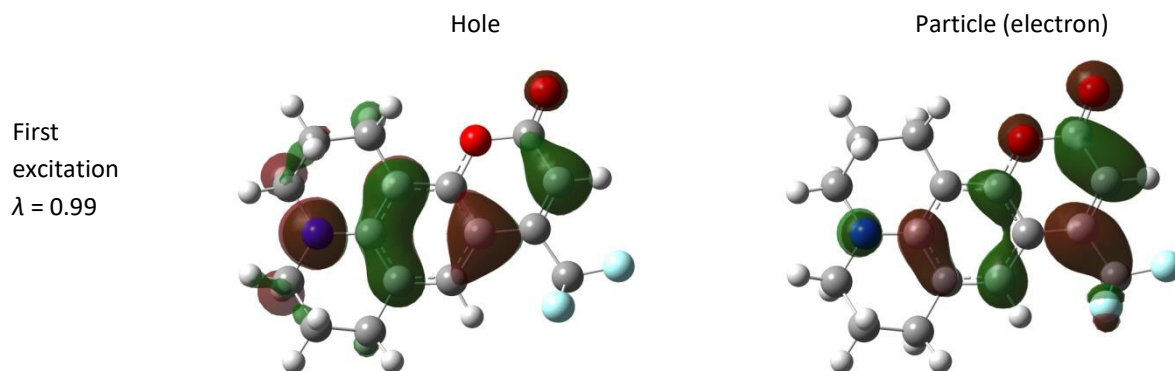


Figure S3 The NTOs of the first vertical excitation of C153 in DMSO at PCM/*m*CAM-B3LYP ($\alpha=0.08$ $\beta=0.92$ $\mu=0.125$)/6-311++G(d,p) level. λ is the contribution of NTO in particular transition.

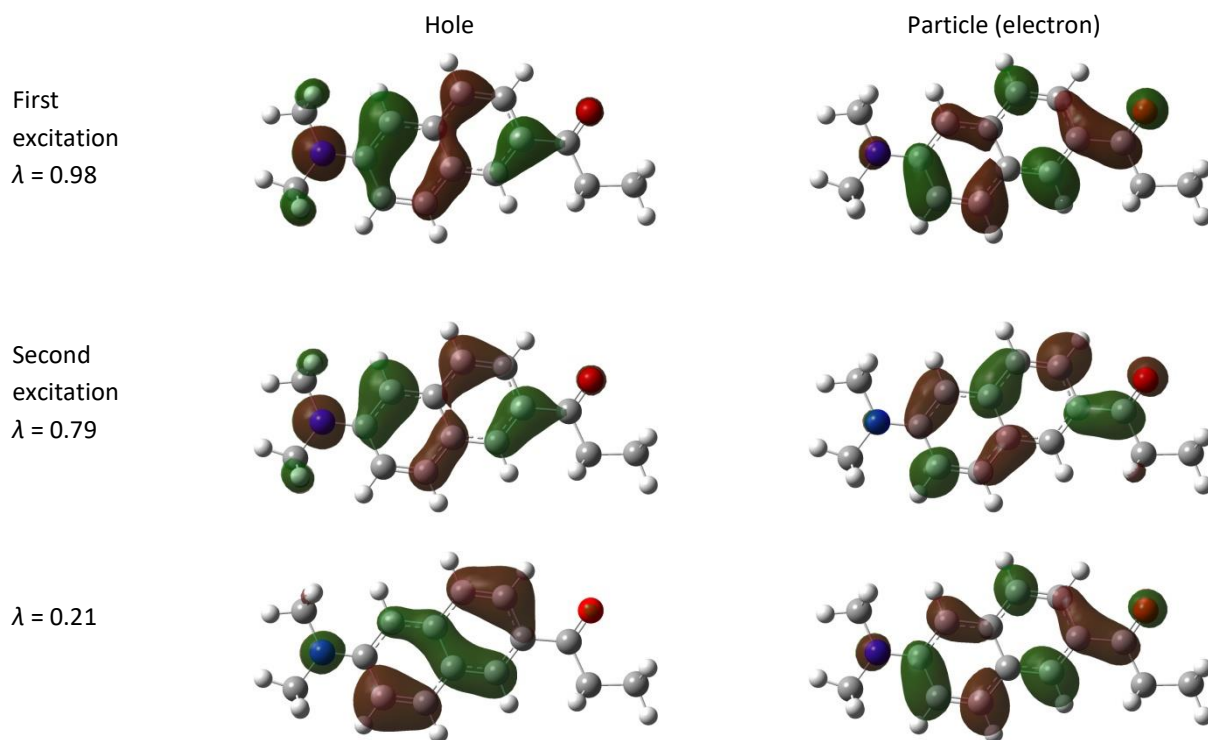


Figure S4 The NTOs of the first two vertical excitations of Prodan in DMSO at PCM/*m*CAM-B3LYP ($\alpha=0.08$ $\beta=0.92$ $\mu=0.15$)/6-311++G(d,p) level. λ is the contribution of NTO in particular transition

$S_0 \rightarrow S_1$ transition of C153 has CT character, the electron density moves from donor (nitrogen and carbon atoms in benzene ring) to acceptor (carbonyl group, oxygen and carbon atoms in pyran ring). The comparison of the NTOs shown in **Figure S3** with canonical molecular orbitals of C153 described by Mühlpfordt *et al.*³¹ reveals that orbitals 80

and 81 in NTO representation closely resemble HOMO and LUMO, respectively. Therefore, the HOMO – LUMO orbital transition provides the dominant contribution to the first singlet excitation in C153.

Prodan has two vertical excitations with non-zero oscillator strengths in the low-energy region. As can be seen from **Figure S4**, the first excitation clearly has CT character, the electron density moves from nitrogen to oxygen. The corresponding one-electron excitation involves transitions from HOMO → LUMO (83.0%) and HOMO → LUMO+1 (13.8%). The NTOs 61 and 62 are similar to HOMO and LUMO, respectively as presented by Alam *et al.*³² The second excitation involves transitions from HOMO → LUMO+1 (64.7%), HOMO-1 → LUMO (22.2%) and HOMO → LUMO (9.2%) and it could be characterized as partial intramolecular charge transfer (ICT) transition.

A comparison of the respective NTOs for the first vertical transition indicates that ICT character for C153 and Prodan is rather different. For Prodan the ICT is quite local; NTOs of C153 show slightly larger extent of ICT. These trends are consistent with the results of calibration where the different optimal values of the range-separating parameter μ in CAM-B3LYP parameter set have been established for C153 and for Prodan.

Experimental 1PA spectra and deconvolution details

The combined symmetric/asymmetric Gaussian deconvolution of the experimental 1PA spectra was used to determine the FWHM of both 1PA and 2PA spectra. The results of Gaussian deconvolution of the experimental 1PA spectra presented in **Figure S5** point to slight differences between the experimental 1PA spectra and those obtained from the peaks of the closest Gaussian curves. For C153, which was initially fitted with three Gaussian functions providing a single asymmetric Gaussian, the 1PA FWHM values are 0.51 eV and 0.47 eV in DMSO and toluene, respectively. Due to more complicated structure of Prodan spectra the well resolved 1PA spectrum measured in cyclohexane was selected as a reference for deconvolution procedure. The spectrum comprises at least two components - a dominant and a minor band represented by three and one Gaussians, respectively. The corresponding fitted 1PA widths are 0.57 and 0.27 eV in DMSO and 0.51 and 0.21 eV in toluene.

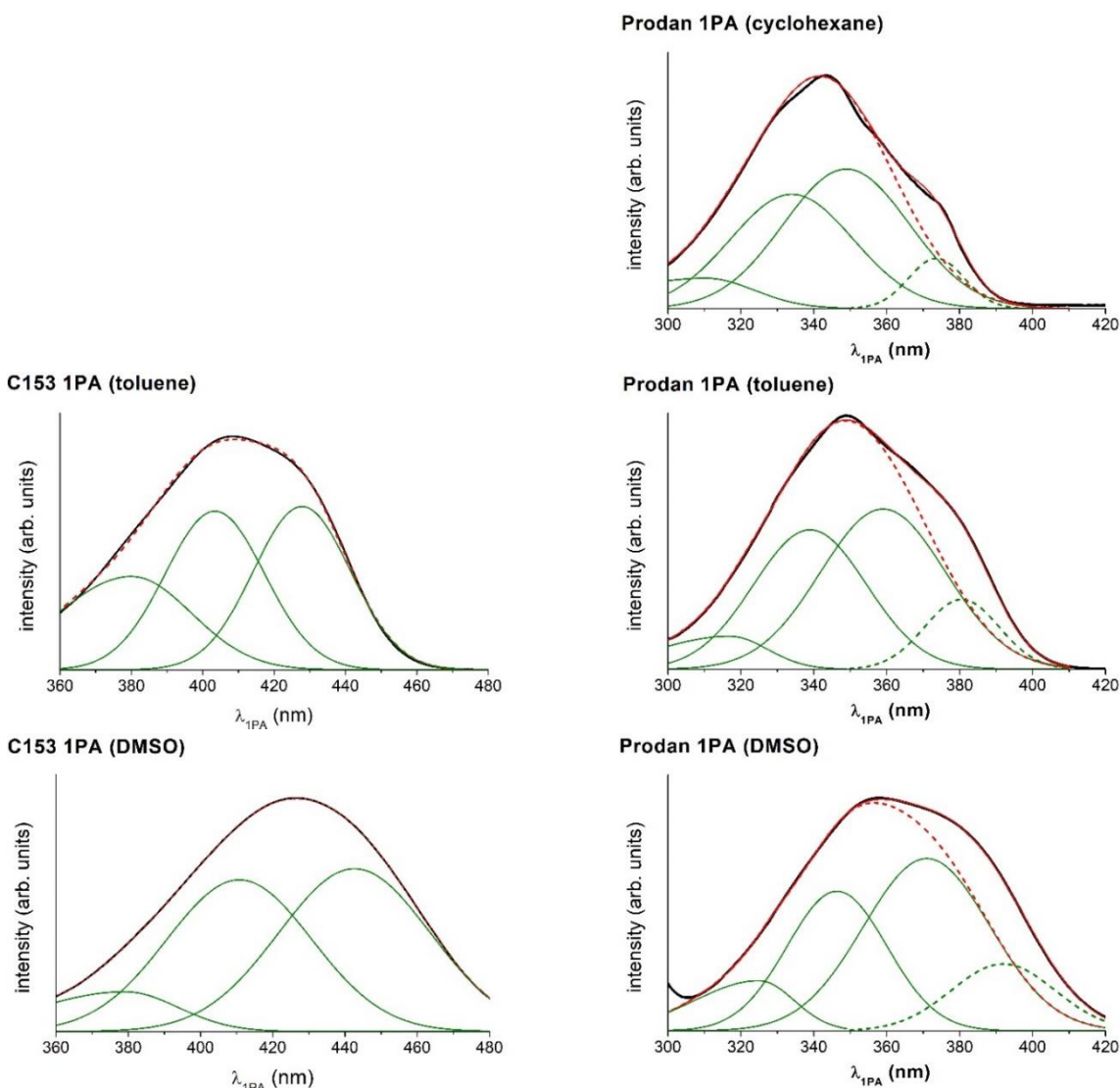


Figure S5 Comparison between the experimental 1PA spectra (black) and spectra from Gaussian deconvolution for C153 (red dashed line) in toluene and DMSO and for Prodan (red line) in toluene and DMSO, respectively. The corresponding contributions were evaluated by fitting the experimental extinction spectrum with a superposition of three bands (green lines) for C153. In case of Prodan the spectrum comprises at least two components - a dominant (red dashed line, represented by three Gaussians) and a minor band (green dashed line).

The results of Gaussian deconvolution of the experimental 2PA spectra are presented in **Figure S6**. 1PA fit parameters were used for fitting experimental 2PA spectra and the 2PA FWHM values are assigned as a half of corresponding 1PA FWHM values.

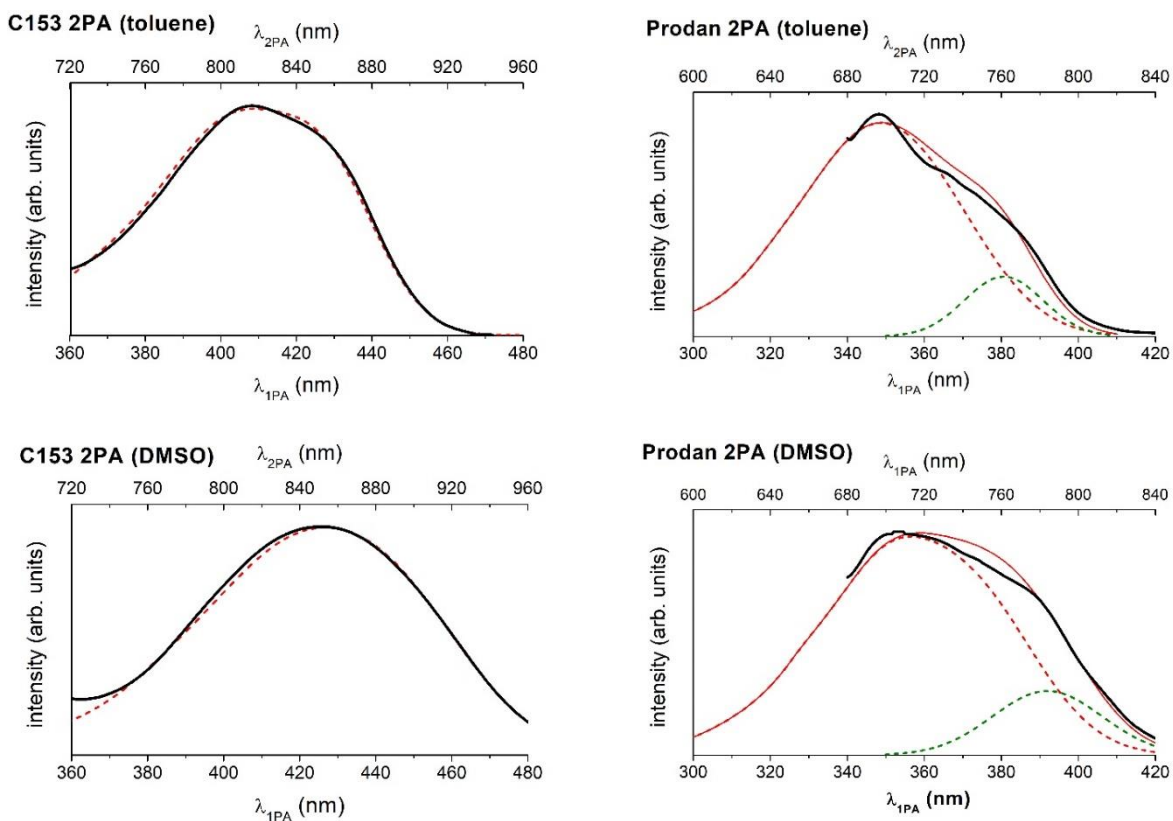


Figure S6 Comparison between the experimental 2PA spectra (black) and spectra from Gaussian deconvolution for C153 (red dashed line) in toluene and DMSO and for Prodan (red line) in toluene and DMSO, respectively. In case of Prodan the corresponding contributions were evaluated by fitting the experimental extinction spectrum with a superposition of two bands (dashed lines).

Vibronic spectra from FCHT calculations

In the present work, the FCHT approximation was used to compare the vibronic band structure with the experimental 1PA spectra in low-energy region. Two values of HWHM were used for convolution of FCHT vibronic spectra by Gaussian broadening function to compare the shapes and positions with corresponding experimental absorption spectrum. According to the data reported by Horng *et al.*³³ the vibronic effects in polar solvents like DMSO should be better accounted for by using the higher value of Gaussian line width selected for convolution as opposed to more narrow line width being appropriate for the solvents of low polarity. In this study the Gaussian functions with HWHM = 300 cm⁻¹ and 600 cm⁻¹ were used to simulate the broadening in toluene. HWHM values of 325 cm⁻¹ and 950 cm⁻¹ were applied for DMSO.

The FCHT spectra were shifted to match the experimental spectra in a similar way as described in Muniz-Miranda *et al.*³⁴ The magnitude of the shift for computed spectra was optimized for the spectrum with larger HWHM value while the convoluted spectrum obtained with smaller value of HWHM provides a good overview of vibronic features of the spectra. It is important to note that using equilibrium solvation contribution for computing relaxed electronic excitations and corresponding adiabatic Hessians, the procedure that is normally implied by FCHT approach, may introduce some deviations from experimental conditions which are probably better aligned with the concept of non-equilibrium solvation. The observed spectral shifts could originate from this misalignment. The computed FCHT spectra and their experimental counterparts are presented in **Figure S7**.

The FCHT calculations bring out the differences in linear spectra. The shape of the calculated FCHT spectrum of C153 in toluene with HWHM 600 cm⁻¹ correctly describes the shape and asymmetry of the corresponding experimental spectrum. Experimental absorption spectrum of Prodan is more complicated due to two vertical excitations in the low-energy band. According to our TD-DFT calculations relying only on the main CT excitation, the vibronic modes of higher intensity are located in the region of experimental absorption maxima and they could be responsible for the expanded shape of the spectra in that region.

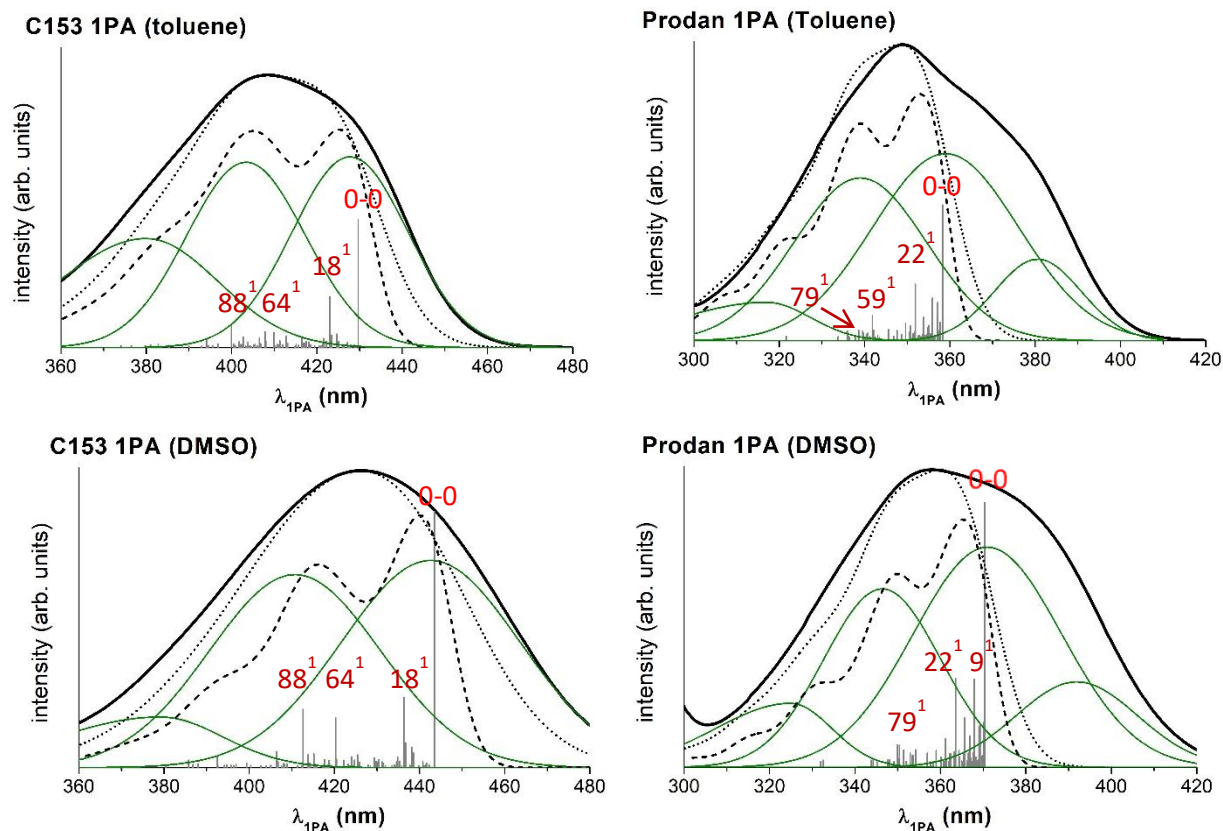


Figure S7 Comparison between the experimental 1PA spectra (black) and stick spectra from FCHT calculations, shifted by -20, -43, -28, and -37 nm for C153 in toluene and DMSO and for Prodan in toluene and DMSO, respectively. Gaussian distribution functions with HWHM = 300 cm^{-1} (dashed line) and 600 cm^{-1} (dotted line) were used to simulate the broadening in toluene and HWHM = 325 cm^{-1} (dashed line) and 950 cm^{-1} (dotted line) in DMSO. The results of the Gaussian deconvolution of the experimental 1PA spectra are also presented (green lines).

The shape of the computed spectra of C153 in DMSO at $\text{HWHM} = 325 \text{ cm}^{-1}$ is similar with the one obtained by Improta *et al.*²⁰ at the PCM/PBE0/6-311+G(d,p) level of theory. However, the set of characteristic vibrational modes is somewhat different. Only the main modes 18^1 and 88^1 are present in both cases (the superscript index stands for the number of quanta associated with the given oscillator). This difference could be attributed to the different choice of the functional and basis set: in the present study we calculated vibronic spectra at PCM/mCAM-B3LYP/6-311++G(d,p) level.

In the present study the following vibrational modes have higher intensities: 18^1 , 64^1 and 88^1 and 9^1 , 22^1 , 59^1 and 79^1 for C153 and Prodan, respectively (see

Figure S7 and **Figure S8**). Modes 18^1 of C153 and 9^1 , 22^1 of Prodan are close to 0-0 transition and can be characterized as a complex motion of the large part of the molecule. In modes 64^1 of C153 and 59^1 of Prodan the dominant displacements represent the bending movement of hydrogen atoms. The stretching motion of the carbonyl group is dominant in modes 88^1 of C153 and 79^1 of Prodan.

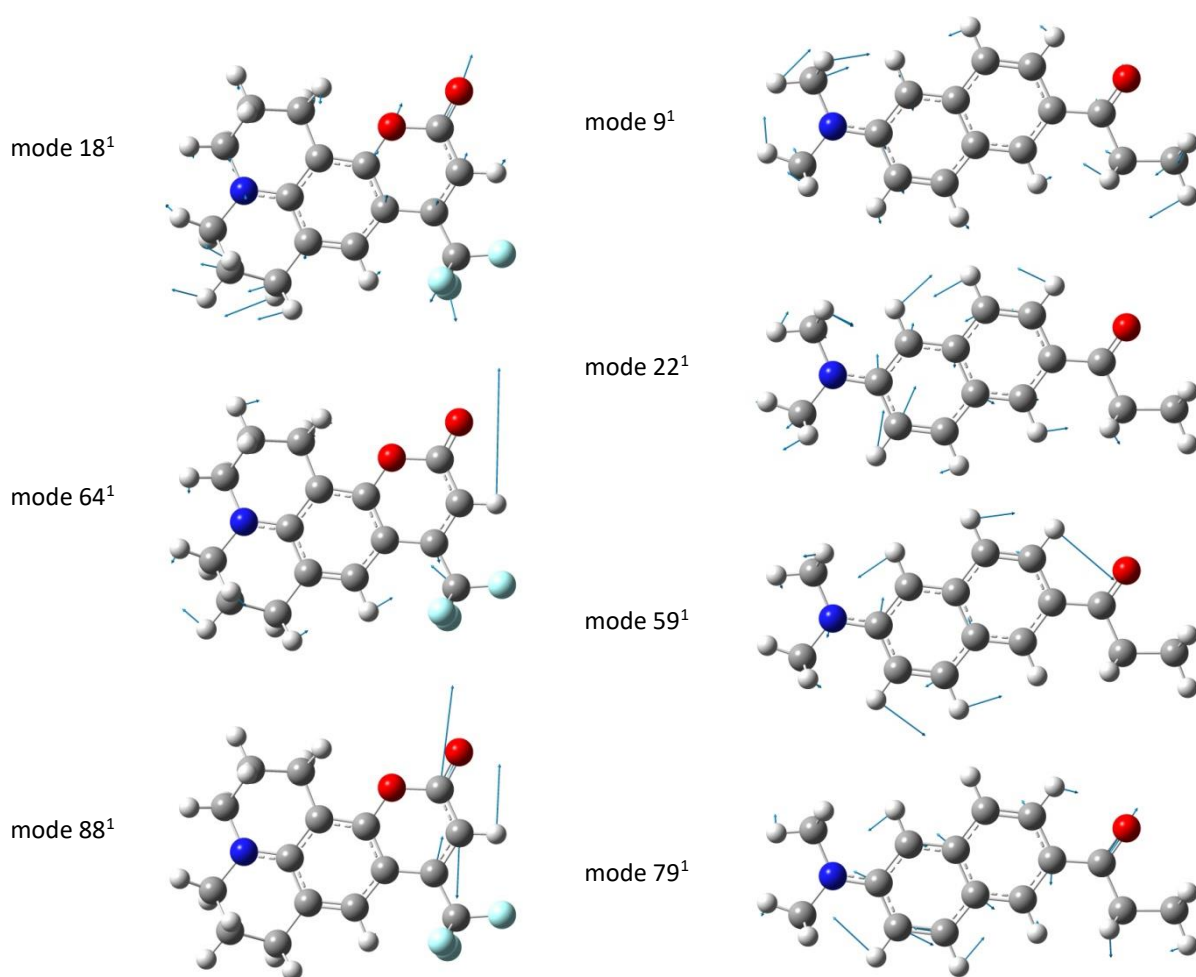


Figure S8 Average direction and magnitude of displacements for the higher intensity modes for C153 (left) and Prodan (right).

For C153 both 64^1 and 88^1 modes shape the second band of the computed FCHT spectra as can be seen from the spectral line constructed with smaller HWHM value. In toluene, it is evident that vibronic couplings determine the

asymmetry of the spectra in the $S_0 \rightarrow S_1$ region (see **Figure S7**). Moreover, in addition to the obvious importance of 64^1 and 88^1 modes the mode 18^1 is providing substantial contribution to the lower energy 0–0 band and these three similar intensity modes could make for the gentle shape of C153 absorption spectra in absorption maxima region. In contrast, for Prodan the asymmetry is due to two separate low-lying electronic excitations as discussed before. Noteworthy, the influence of carbonyl group stretching on C153 spectra (mode 88^1) is higher than its influence on Prodan spectra (mode 79^1).

In toluene the experimental 1PA spectral lines are narrow and sharp-angled; in DMSO the absorption spectra are extended and have relatively smooth shape. It is important to note that these spectral shapes in toluene and DMSO are reasonably reflected in the results of the calculations of vibronic spectra. For example, the range of the stick spectra of C153 is 55.6 nm and 63.2 nm in toluene and DMSO, respectively.

The comparison of Gaussian deconvolution of the experimental 1PA spectra with the FCHT spectrum obtained with smaller HWHM value provides further details on the experimental line shapes. It appears that for C153 the energy of $S_0 \rightarrow S_1$ 0-0 excitation and the first vibronic band matches the low energy shoulder of experimental spectra. The wavelengths of computational 0-0 component of $S_0 \rightarrow S_1$ transitions after appropriate shift and the first peak of deconvoluted experimental spectra (the value given in parentheses) for C153 are 430 nm (431 nm) and 444 nm (447 nm) in toluene and DMSO, respectively. The other vibronic bands are also in good agreement with the peak positions of deconvoluted spectra. In contrary, for Prodan the vibronic features of the 0-0 band of the calculated spectra are too distant to provide the reasonable match with experimentally observed low energy shoulder. However, the vibronic bands of FCHT spectra provide accurate description of the maximum absorption region of the experimental low-energy band and the corresponding high-energy shoulder. For the low-energy shoulder of this absorption band no match can be established from TD-DFT approach.

Fluorescence excitation anisotropy of Prodan

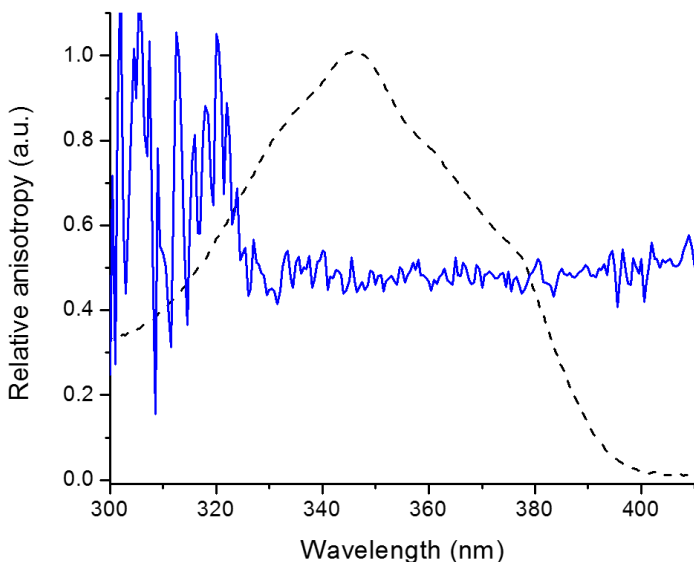


Figure S9. Blue solid line – relative fluorescence excitation anisotropy of Prodan in polyethylene film at RT. Dashed black line – normalised to peak linear absorption spectrum.

The fluorescence excitation anisotropy of Prodan was measured by embedding the dye into a solid polyethylene (PE) film and measuring the fluorescence at 420 nm as a function of the excitation wavelength (both excitation and emission spectral width 2.5 nm) using PerkinElmer LS 50B spectrofluorometer. The excitation polarizer was set to vertical polarization and the fluorescence detection channel polarizer was set to vertical and horizontal direction. Due to lack of the calibration of the fluorescence detection channel for the two polarizations, the anisotropy is presented in relative units only. Nevertheless, the flat trend of the fluorescence anisotropy between 330 and 400 nm indicates that the angle between the absorption and fluorescence dipole moments is essentially constant in this spectral range. Increased noise at wavelengths <320 nm is due to a low transmittance of the excitation polarizer at the shorter wavelengths.

REFERENCES

- 1 A. Rebane, G. Wicks, M. Drobizhev, T. Cooper, A. Trummal and M. Uudsemaa, *Angew. Chem. Int. Ed.*, 2015, **54**, 7582–7586.
- 2 A. D. Becke, *J. Chem. Phys.*, 1993, **98**, 5648–5652.
- 3 C. Lee, W. Yang and R. G. Parr, *Phys. Rev. B*, 1988, **37**, 785–789.
- 4 M. J. Frisch, J. A. Pople and J. S. Binkley, *J. Chem. Phys.*, 1984, **80**, 3265–3269.
- 5 E. Cancès, B. Mennucci and J. Tomasi, *J. Chem. Phys.*, 1997, **107**, 3032–3041.
- 6 B. Mennucci, E. Cancès and J. Tomasi, *J. Phys. Chem. B*, 1997, **101**, 10506–10517.
- 7 M. J. Frisch, G. W. Trucks, H. B. Schlegel, G. E. Scuseria, M. A. Robb, J. R. Cheeseman, G. Scalmani, V. Barone, B. Mennucci, G. A. Petersson, H. Nakatsuji, M. Caricato, X. Li, H. P. Hratchian, A. F. Izmaylov, J. Bloino, G. Zheng, J. L. Sonnenberg, M. Hada, M. Ehara, K. Toyota, R. Fukuda, J. Hasegawa, M. Ishida, T. Nakajima, Y. Honda, O. Kitao, H. Nakai, T. Vreven, J. A. Montgomery Jr., J. E. Peralta, F. Ogliaro, M. Bearpark, J. J. Heyd, E. Brothers, K. N. Kudin, V. N. Staroverov, R. Kobayashi, J. Normand, K. Raghavachari, A. Rendell, J. C. Burant, S. S. Iyengar, J. Tomasi, M. Cossi, N. Rega, J. M. Millam, M. Klene, J. E. Knox, J. B. Cross, V. Bakken, C. Adamo, J. Jaramillo, R. Gomperts, R. E. Stratmann, O. Yazyev, A. J. Austin, R. Cammi, C. Pomelli, J. W. Ochterski, R. L. Martin, K. Morokuma, V. G. Zakrzewski, G. A. Voth, P. Salvador, J. J. Dannenberg, S. Dapprich, A. D. Daniels, Ö. Farkas, J. B. Foresman, J. V. Ortiz, J. Cioslowski and D. J. Fox, *Gaussian 09 Revision B.01*, Gaussian Inc. Wallingford CT, 2009.
- 8 K. Aidas, C. Angeli, K. L. Bak, V. Bakken, R. Bast, L. Boman, O. Christiansen, R. Cimraglia, S. Coriani, P. Dahle, E. K. Dalskov, U. Ekström, T. Enevoldsen, J. J. Eriksen, P. Ettenhuber, B. Fernández, L. Ferrighi, H. Fliegl, L. Frediani, K. Hald, A. Halkier, C. Hättig, H. Heiberg, T. Helgaker, A. C. Hennum, H. Hettema, E. Hjertenæs, S. Høst, I.-M. Høyvik, M. F. Izzi, B. Jansik, H. J. Aa. Jensen, D. Jonsson, P. Jørgensen, J. Kauczor, S. Kirpekar, T. Kjærgaard, W. Klopper, S. Knecht, R. Kobayashi, H. Koch, J. Kongsted, A. Krapp, K. Kristensen, A. Ligabue, O. B. Lutnæs, J. I. Melo, K. V. Mikkelsen, R. H. Myhre, C. Neiss, C. B. Nielsen, P. Norman, J. Olsen, J. M. H. Olsen, A. Osted, M. J. Packer, F. Pawłowski, T. B. Pedersen, P. F. Provasi, S. Reine, Z. Rinkevicius, T. A. Ruden, K. Ruud, V. V. Rybkin, P. Sałek, C. C. M. Samson, A. S. de Merás, T. Saue, S. P. A. Sauer, B. Schimmelpfennig, K. Sneskov, A. H. Steindal, K. O. Sylvester-Hvid, P. R. Taylor, A. M. Teale, E. I. Tellgren, D. P. Tew, A. J. Thorvaldsen, L. Thøgersen, O. Vahtras, M. A. Watson, D. J. D. Wilson, M. Ziolkowski and H. Ågren, *WIREs Comput Mol Sci*, 2014, **4**, 269–284.
- 9 *Dalton, a molecular electronic structure program, Release Dalton*, 2015.
- 10 C. Adamo and V. Barone, *J. Chem. Phys.*, 1999, **110**, 6158–6170.
- 11 T. Yanai, D. P. Tew and N. C. Handy, *Chem. Phys. Lett.*, 2004, **393**, 51–57.
- 12 E. Runge and E. K. U. Gross, *Phys. Rev. Lett.*, 1984, **52**, 997–1000.
- 13 K. A. Nguyen, P. N. Day and R. Pachter, *J. Chem. Phys.*, 2007, **126**, 094303.
- 14 M. G. Vivas, D. L. Silva, J. Malinge, M. Boujtita, R. Zalesny, W. Bartkowiak, H. Ågren, S. Canuto, L. D. Boni, E. Ishow and C. R. Mendonca, *Sci. Rep.*, 2014, **4**, 4447.
- 15 D. Shcherbin and K. Ruud, *Chem. Phys.*, 2008, **349**, 234–243.
- 16 D. Jacquemin, E. A. Perpète, G. E. Scuseria, I. Ciofini and C. Adamo, *J. Chem. Theory Comput.*, 2008, **4**, 123–135.
- 17 D. Jacquemin, V. Wathelet, E. A. Perpète and C. Adamo, *J. Chem. Theory Comput.*, 2009, **5**, 2420–2435.
- 18 A. Charaf-Eddin, A. Planchat, B. Mennucci, C. Adamo and D. Jacquemin, *J. Chem. Theory Comput.*, 2013, **9**, 2749–2760.
- 19 K. Okuno, Y. Shigeta, R. Kishi, H. Miyasaka and M. Nakano, *J. Photochem. Photobiol. Chem.*, 2012, **235**, 29–34.
- 20 R. Improta, V. Barone and F. Santoro, *Angew. Chem.*, 2007, **119**, 409–412.
- 21 A. Pedone, J. Bloino and V. Barone, *J. Phys. Chem. C*, 2012, **116**, 17807–17818.
- 22 F. Santoro, R. Improta, A. Lami, J. Bloino and V. Barone, *J. Chem. Phys.*, 2007, **126**, 084509.
- 23 O. Christiansen, H. Koch and P. Jørgensen, *Chem. Phys. Lett.*, 1995, **243**, 409–418.
- 24 C. Hättig and F. Weigend, *J. Chem. Phys.*, 2000, **113**, 5154–5161.
- 25 F. Weigend, M. Häser, H. Patzelt and R. Ahlrichs, *Chem. Phys. Lett.*, 1998, **294**, 143–152.
- 26 F. Weigend and R. Ahlrichs, *Phys. Chem. Chem. Phys.*, 2005, **7**, 3297–3305.
- 27 A. Hellweg, C. Hättig, S. Höfener and W. Klopper, *Theor. Chem. Acc.*, 2007, **117**, 587–597.
- 28 N. Nakatsuji, *Chem. Phys. Lett.*, 1978, **59**, 362–364.
- 29 H. Nakatsuji, *Chem. Phys. Lett.*, 1979, **67**, 329–333.
- 30 *TURBOMOLE V6.4 2012*, a development of University of Karlsruhe and Forschungszentrum Karlsruhe GmbH, 1989–2007, TURBOMOLE GmbH, since 2007; available from <http://www.turbomole.com>, 2012.

- 31 A. Mühlpfordt, R. Schanz, N. P. Ernsting, V. Farztdinov and S. Grimme, *Phys. Chem. Chem. Phys.*, 1999, **1**, 3209–3218.
- 32 M. M. Alam and M. Chattopadhyaya, *J. Chem. Sci.*, 2014, **126**, 1217–1226.
- 33 M. L. Horng, J. A. Gardecki, A. Papazyan and M. Maroncelli, *J. Phys. Chem.*, 1995, **99**, 17311–17337.
- 34 F. Muniz-Miranda, A. Pedone, G. Battistelli, M. Montalti, J. Bloino and V. Barone, *J. Chem. Theory Comput.*, 2015, **11**, 5371–5384.